Supporting Information

Ultrafast Dissolution of Intact Wood via Deep Eutectic Solvent-Mediated Pathways

Enqing Zhu[a,#], Lili Zhang[a,#], Qing Zhang[a], Shaoning Wang[a], Xin Li[a], Zhengjun Shi[b], Jinxia Ma[a], Juan Yu[a], Muhammad Wajid Ullah[a], Khalid Ali Khan[c], Zhiguo Wang[a,*], Yimin Fan[a,*], Orlando·J·Rojas[d]

[a] Jiangsu Co-Innovation Center of Efficient Processing and Utilization of Forest Resources, International Innovation Center for Forest Chemicals and Materials, College of Light Industry and Food Engineering, College of Chemical Engineering, Nanjing Forestry University, Nanjing 210037, China

[b] University Key Laboratory of Biomass Chemical Refinery & Synthesis, Southwest Forestry University, Kunming 650224, China

[c] Applied College, Research Center for Advanced Materials Science, King Khalid University, Abha 61413, Saudi Arabia

[d] Bioproducts Institute, Department of Chemical and Biological Engineering, Department of Chemistry and Department of Wood Science, University of British Columbia Vancouver, British Columbia V6T 1Z4, Canada

***Correspondence:** College of Light Industry and Food Engineering, Longpan Road 159, Nanjing Forestry University, Nanjing 210037, China (Z. Wang). College of Chemical Engineering, Longpan Road 159, Nanjing Forestry University, Nanjing 210037, China (Y. Fan).

E-mail addresses: wzg@njfu.edu.cn (Z. Wang), fanyimin@njfu.edu.cn (Y. Fan)

# These authors contributed equally to this work.

Characterization

The swelling degree of the wood cell. The morphological evolution of wood cell walls before and after swelling in the $ZnCl_2$-LA DES was examined using environmental scanning electron microscopy (ESEM, Quanta 200, FEI, USA). To ensure experimental reproducibility and statistical reliability, five independent parallel samples were prepared for each swelling condition. For each sample, ESEM images were analyzed using Nano Measurer software. The cell wall thickness was quantified by measuring the distance between two adjacent cell lumens (lumen-to-lumen distance), which represents the total thickness of the double cell wall, including the S1, S2, and S3 layers of both neighboring cells as well as the intervening middle lamella. Measurements were taken at no fewer than 50 distinct positions across different regions of the cell wall to minimize local heterogeneity. The average cell wall thickness and corresponding standard deviation were calculated for each treatment, and the swelling degree was subsequently determined according to the defined equation.

The distribution of Zn in the cell wall was analyzed with energy-dispersive X-ray spectroscopy (EDS, Quanta 200, FEI, USA). The swelling degree of the cell wall is calculated according to equation (1):

$$Swelling\ degree = \frac{C_2 - C_1}{C_1} \times 100\% \quad (1)$$

Where C_2 is the lumen-to-lumen distance (i.e., the total thickness of the double cell wall, including the S1, S2, and S3 layers of two adjacent cells as well as the middle lamella) after swelling in the $ZnCl_2$-LA DES, and C_1 is the corresponding lumen-to-lumen distance of the native wood before swelling.

Structural and physicochemical characterizations. Crystalline and nanoscale structures of Wood, SWood were analyzed using wide-angle X-ray scattering (WAXS, 5-30 nm^{-1}) and small-angle X-ray scattering (SAXS, 0.08-5 nm^{-1}), respectively (CuKα, λ = 0.154 nm, SAXSpoint 5.0, Anton Paar, Graz, Austria). Samples (diameter=2 mm, thickness=1 mm) were used for the measurements. The samples were placed in the cellulose fiber direction perpendicular to the incident beam. The sample-to-detector distances for WAXS and SAXS were 89 mm and 700 mm, respectively. The obtained two-dimensional patterns were analyzed using the SAXS analysis software, in which they were transformed into one-dimensional diffractograms. The distance between cellulose microfibrils (d) was calculated using the following equation[1] (2):

$$d = \frac{2\pi}{q} \tag{2}$$

where q is the scattering angle of the intensity peak.

Light microscopy. The wood dissolution process was observed with an optical microscope (Nikon E100, Shanghai Optoelectronics Technology Co., Ltd.). The magnification used was 400× (40×10).

Viscosity of wood solution. The rheological properties of cellulose solution were measured at 25 ℃ and angular frequencies ranging from 0.1 to 100 rad using a P35/1° TiL cone-plate of Thermo Scientific HAAKE RheoStress6000 (USA).

The transparency of the wood solution. The transparency of the wood solutions was evaluated using a UV-visible spectrophotometer (TU-1810, Persee, China). The transmittance of the solution samples was recorded in the wavelength range of 400-700 nm at room temperature.

Morphology and chemical structure. Additionally, the morphology of the regenerated wood was observed using a field-emission scanning electron microscope (FE-SEM, JSM-7600F, Japan) at an accelerated voltage of 5-10 kV. The degree of polymerization of cellulose in the wood before swelling, after swelling, and after regeneration was determined by measuring intrinsic viscosity in a copper ethylenediamine solution, using the Mark-Houwink-Sakurada equation[2]. The crystal structures of all samples were characterized by X-ray diffraction (XRD, Bruker D8 ADVANCE, Germany) at 40 kV and 30 mA, with diffraction angles ranging from 2θ = 5° to 40° and a scan rate of 5°/min. The crystallinity index was calculated using the Segal method[3]. Fourier transform infrared (FTIR) spectroscopy was conducted on Wood, SWR samples, and RWood in the wavenumber range of 4000 to 400 cm^{-1} (Thermo Scientific Nicolet iS5 with iD7 ATR accessory, USA).

(Bio-)chemical content. The residual amounts of cellulose, hemicellulose, and lignin in the wood after DES swelling were assessed using the NREL method[4]. A sample of 0.3 g of absolute dry solid was mixed with 3 mL of 72% H_2SO_4 and placed in a pressure vessel to soak for 1 h. Afterward, 84 mL of ultrapure water was added, and the mixture was hydrolyzed for 1 h in a steam sterilizer (BKQ-B75II, Shandong Brock Disinfection Equipment Co., Ltd., Jinan, China) at 121 °C. Monosaccharide concentrations in the resulting liquid were measured using the Ultimate 3000 high-performance liquid chromatography (HPLC) system, equipped with a separation column (Aminex HPX-87H, Bio-Rad, CA, USA) and a differential refractive index detector (RID-20A, Shimadzu, Japan).

Compositional analysis of hydrolysate.

The liquid fractions obtained after wood dissolution in the $ZnCl_2/H_2O$/LA system under different conditions were separated by centrifugation at 8000 rpm for 10 min to remove insoluble residues. The collected supernatants were diluted appropriately with deionized water to minimize matrix effects and ensure accurate chromatographic analysis. Soluble monosaccharides and oligosaccharides derived from hemicellulose were quantified directly from the centrifuged $ZnCl_2/H_2O$/LA solutions without any acid hydrolysis. Monosaccharides were analyzed by high-performance liquid chromatography (HPLC, Agilent 1260) equipped with a refractive index detector and an Aminex HPX-87H column (300 × 7.8 mm, Bio-Rad). The mobile phase was 5 mM H_2SO_4 at a flow rate of 0.6 mL·min^{-1}, the column temperature was maintained at 55 °C, and the injection volume was 10 μL. External calibration was performed using xylose standards. Xylo-oligosaccharides (X2-X6) present in the solutions were directly determined by high-performance anion-exchange chromatography with pulsed amperometric detection (HPAEC-PAD, Thermo Dionex ICS-5000, USA) using a CarboPac PA200 column (3 × 250 mm) with a PA200 guard column (3 × 50 mm). Eluent A was 100 mM NaOH, and eluent B was 100 mM NaOH containing 500 mM sodium acetate. Gradient elution was carried out at a flow rate of 0.3 mL·min^{-1}, column temperature of 30 °C, and an injection volume of 10 μL. Quantification was achieved using external calibration with X2-X6 standards. The yields of soluble monosaccharides and oligosaccharides were calculated based on the initial hemicellulose content of the raw biomass according to previously reported methods[5].

X-ray photoelectron spectroscopy. Changes in Wood and SWR surface functional groups were analyzed using X-ray photoelectron spectroscopy (XPS), with C1s data fitted using XPS Peak Fit software (XPSPEAK41, Raymund Kwok).

Fully automatic specific surface area and porosity analysis. The SWR was freeze-dried to obtain the final sample. To remove moisture, the sample was degassed at 110 ℃ for 8 h before being replaced on the analyzer for further analysis at 77K. Surface area and pore size distribution were determined using a V-Sorb 2800P analyzer. Specific surface area and pore size distribution were calculated using the Barrett-Joyner-Halenda (BJH) and Brunauer-Emmet-Teller (BET) methods under varying relative pressures.

Thermogravimetric analysis. The thermal stability of the wood before and after regeneration was evaluated with a thermogravimetric analyzer (TGA, HCT-1/2, HENVEN-HJ, China). Samples weighing 10-20 mg were heated from 25 ℃ to 600 ℃ at a scan rate of 10 ℃/min in a ceramic crucible under a N_2 atmosphere.

Molecular weights. The Molecular weights *(M_w)* of MWL and SWL was determined by gel permeation chromatography (GPC, Agilent 1200 Series, Santa Clara, CA) using a Waters 2410 refractive index detector (RID) and a Mono-GPC analytical column.

^{1}H-^{13}C two-dimensional NMR. The structure of lignin was characterized by ^{1}H-^{13}C two-dimensional NMR (2D HSQC NMR) using a Bruker 600 MHz instrument (AVANCE III, Switzerland) equipped with a low-temperature-cooled 5-mm TCI z-gradient triple resonance probe. Following a previously reported method (Kim et al.,

2008), 50 mg lignin was dissolved in 0.5 mL of DMSO-d_6 solvent. The chemical shift ranges for ^{1}H and ^{13}C were 0-16 ppm (9615 Hz) and 0-165 ppm (24900 Hz), respectively. The data were collected over 1 h with 2048 complex points, a recovery delay of 1.5 s, and 64 transient numbers with 256 time increments for the ^{13}C dimension. Chemical shifts were calibrated using DMSO (δ_C 39.5 ppm, δ_H 2.5 ppm) [6].

^{31}P nuclear magnetic resonance. Quantitative ^{31}P nuclear magnetic resonance (NMR) analysis was performed to determine the content and distribution of hydroxyl groups in lignin[7]. Accurately weighed freeze-dried lignin samples (50.0 mg) were dissolved in 500 μL of anhydrous pyridine/deuterated chloroform (1.6:1.0, v/v) under stirring. After complete dissolution, 100 μL of cyclohexanol internal standard solution (10.85 mg mL^{-1} in the same solvent mixture) and 100 μL of chromium(III) acetylacetonate solution (5 mg mL^{-1}, used as a relaxation reagent) were added. Subsequently, 100 μL of 2-chloro-4,4,5,5-tetramethyl-1,3,2-dioxaphosphorane (TMDP) was rapidly introduced for derivatization. The NMR spectra of freshly prepared samples were recorded at room temperature using a Bruker AVII 600 MHz spectrometer equipped with a QNP cryoprobe. Chemical shifts were referenced to the phosphorylation product of TMDP with trace moisture in the sample, which produced a sharp and stable signal at 132.2 ppm.

Differential Scanning Calorimetry (DSC). The freezing points of the solvents were determined using a differential scanning calorimeter (DSC 214 Polyma, NETZSCH, Germany). Approximately 15-20 mg of each sample was sealed in an aluminum pan. The samples were first cooled to -130 °C at a rate of 10 °C min^{-1} and held isothermally for 3

min. Subsequently, they were heated to 25 °C at the same rate, and the heating segment of the thermogram was used for data analysis.

Low-field nuclear magnetic resonance. Using low field nuclear magnetic resonance spectrometer (VTMR20-010-T Niumag China) at room temperature measuring solvent 1 h low field nuclear magnetic resonance (NMR) spectra of the solvent Used to reflect the different state of water in the solvent.

Molecular dynamics simulations

The molecular dynamics (MD) simulations were carried out using Material Studio (MS, version 2020) from Accelrys, Inc[8]. The classical MD simulations were performed with the Forcite module in MS., and the COMPASS II force field was used to model interactions between plant fiber and solvents[9]. The initial configuration of the solvents was prepared using the Amorphous Cell tool in MS. The system consisted of a 4 × 4 × 4 nm cubic box containing 50 $ZnCl_2$ molecules, 100 H_2O molecules, 10 lactic acid molecules, and 1 molecule of either lignin or cellulose 66. The Ewald summation method was employed to calculate the Coulombic interactions, with an accuracy of 0.0001 kcal/mol and a cutoff distance of 15.5Å. Temperature control was maintained using the Nosé method, while pressure and particle number were controlled with the Berendsen method NPT (constant particle number, pressure, and temperature) dynamics[10, 11] A total simulation time of 5.0 ns was used, with a timestep of 1.0 fs to typical production MD runs.

The interaction energies between solvents ($Z_1H_2L_{0.2}$, $Z_1H_3L_{0.2}$, and $Z_1H_5L_{0.2}$) and various components (cellulose and lignin) in the plant fibers solution were calculated.

In the A–B system, component A refers to the solvent ($Z_1H_2L_{0.2}$, $Z_1H_3L_{0.2}$, and $Z_1H_5L_{0.2}$), while component B refers to a biomass component (cellulose or lignin). For the A & B system, the interaction energy (ΔE) was determined using the following formula:

$$\Delta E = E_{AB} - (E_A + E_B)$$

Where E_{AB} is the total energy of the system, E_A is the energy of component A, and E_B is the energy of component B[12, 13].

Mechanical property： The mechanical properties of the samples were measured using a TRAPEZIUM X tensile testing system (Shimadzu Corporation, Japan). The samples were stretched at a rate of 5 mm min^{-1}, and the tensile stress and strain were recorded. Each set of samples was tested eight times, and the average values and standard deviations were calculated.

The heat insulation performance of Regenerated wood aerogel. The thermal insulation performance of the regenerated wood aerogel was evaluated using a DS-2TPH10-3AUF handheld thermal imaging camera (Hikvision, China)**.** The temperature variations on the surface of the regenerated wood aerogel were recorded during the measurement.

Table S1. Calculation of the energy consumption, efficiency and yield of dissolution of wood.

Method	Sample	Procedure	**Pretreatment**			**Dissolution**						**Total**				**Ref.**
						Stirring			Heating			Yield	Energy	Energy consumption	Energy efficiency	
			Powers [W]	Time [h]	Energy [kJ]	Powers [W]	Time [h]	Energy [kJ]	Powers [W]	Time [h]	Energy [kJ]	[%]	[kJ]	[kJ/g]	[g/ kJ]	
$Z_1H_3L_{0.2}$	Wood	Heating	600	1	2160	25	1.5	1350	\	\	\	70	3510	5.01	0.20	This work
LiCl/DMSO	Wood	Ball-milling	1500	2	16200	25	24	21600	\	\	\	93	37800	37.80	0.026	[14]
[Bmim]Cl [Amim]Cl	Wood	\	\	\	\	25	8	7200	600	8	17280	91	24480	24.48	0.041	[15]
EmimOAc / EA-DBN	Corncob	Ball-milling	1500	4	21600	25	5	4500	600	5	10800	65	36900	56.64	0.018	[16]
[C2mim]OAc	Wood	\	\	\	\	25	16	14400	600	16	34560	62	48960	78.97	0.013	[17]
α-keto acid	Wood	Ball-milling	1500	48	259200	25	24	21600	\	\	\	73	280800	384.66	0.0026	[18]

a) Powers was calculated by total consumption for the treatment of wood (1 kg); b) Time was obtained from the preparation process (wood 1 kg); c)Energy consumption = Energy/(1000 × Yield) d)Energy efficiency = 1000/Energy consumption

Table S2 Assignment of main lignin and carbohydrates ^{13}C single bond ^{1}H correlation peaks in the HSQC spectra of MWL and SWL.

Labels	**δC/δH (ppm)**	**Assignment**
OMe	55.4/3.72	C-H in methoxyls
A_γ	59.6/3.29-3.85	C_γ-H_γ in β-*O*-4 substructures
A'_γ	62.9/4.44	C_γ-H_γ in γ-acylated β-*O*-4
C_γ	62.2/3.71	C_γ-H_γ in phenylcoumaran
B_γ	70.8/3.81-4.15	C_γ-H_γ in β-β resinol
$S_{2,6}$	103.5/6.67	$C_{2,6}$-$H_{2,6}$ in syringyl units
$S'_{2,6}$	106.1/7.22	$C_{2,6}$-$H_{2,6}$ in oxidized S units
G_2	110.0/6.97	C_2-H_2 in guaiacyl units
G_5	114.8/6.8	C_5-H_5 in guaiacyl units
G_6	118.8/6.76	C_6-H_6 in guaiacyl units
PB	130.7/7.66	$C_{2,6}$-$H_{2,6}$ in p-coumarate

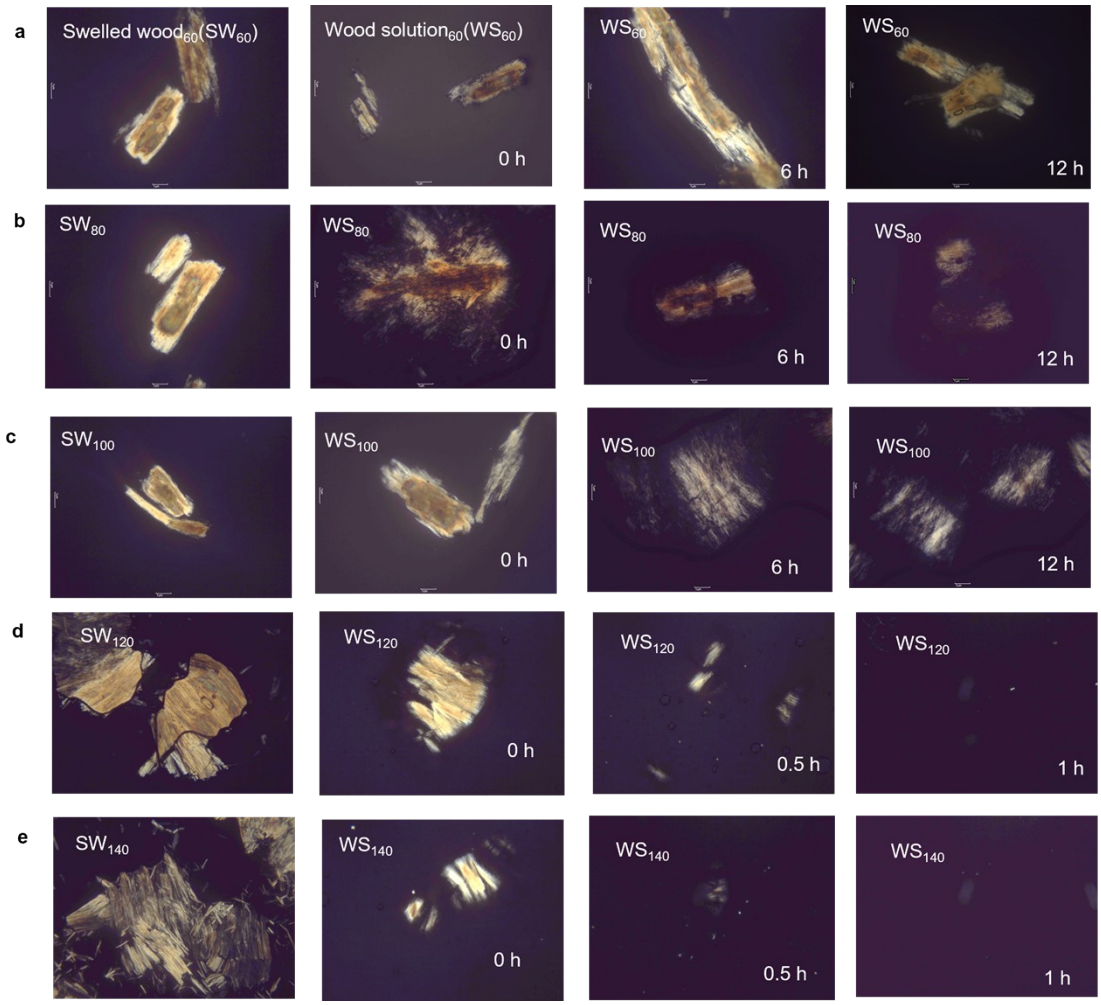

Fig. S1. The effect of the swelling temperature on the dissolution of wood in $Z_1H_3L_{0.2}$. Optical micrographs show the effect of wood swelling in $ZnCl_2$-LA DES with different temperature ((a) 60 °C, (b) 80 °C, (c) 100 °C, (d) 120 °C, and (e) 140 °C) on its dissolution behavior in $ZnCl_2 \cdot 3H_2O$ for different time. When the swelling temperature was adjusted to 120 °C, the wood was completely dissolved within 1 h, forming a homogeneous wood solution.

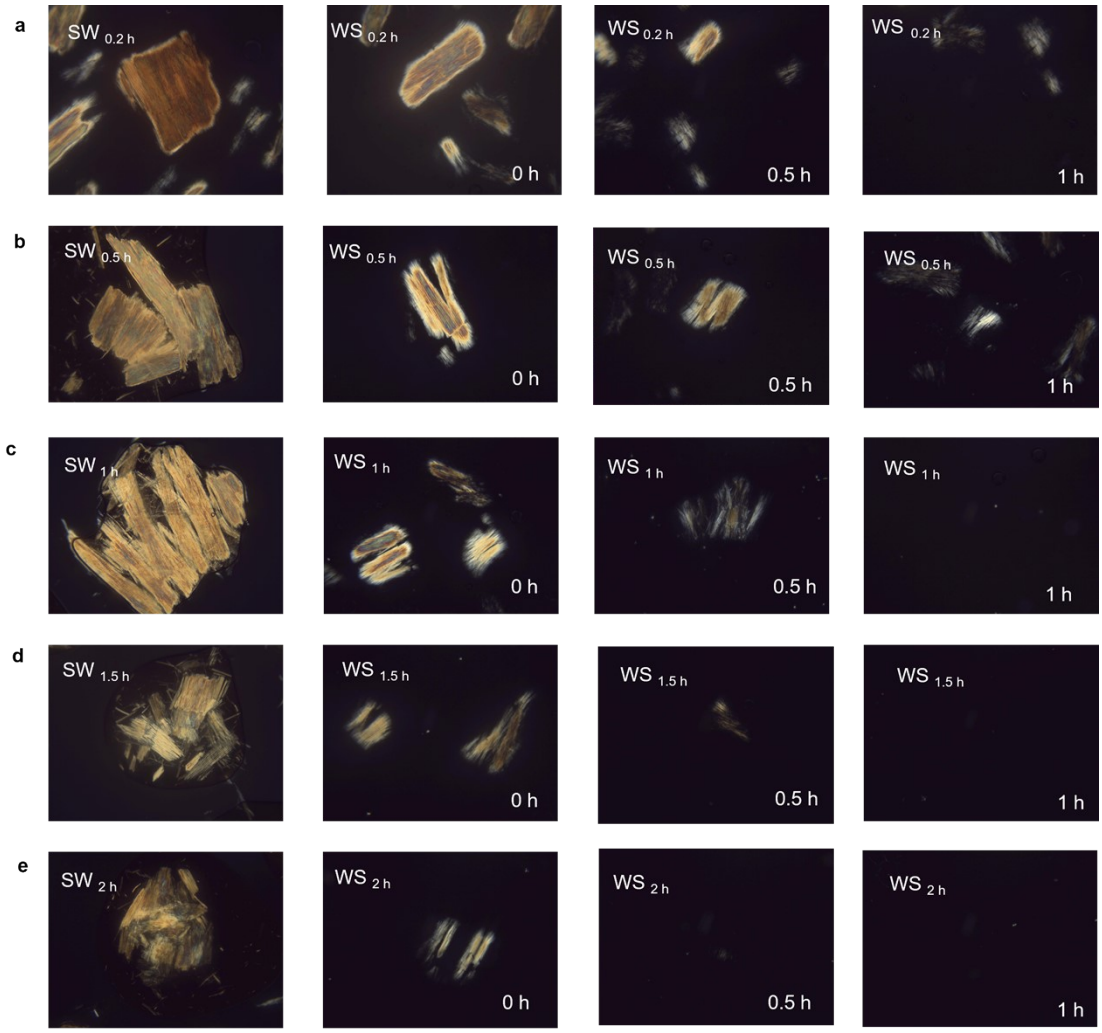

Fig. S2. The effect of the swelling time on the dissolution of wood in $Z_1H_3L_{0.2}$. Optical micrographs show the effect of wood swelling in $ZnCl_2$-LA DES with different time ((a)0.2 h, (b) 0.5 h, (c) 1 h, (d) 1.5 h, and (e)2 h) on its dissolution behavior in $ZnCl_2 \cdot 3H_2O$ for different time. When the swelling time was adjusted to 1h, the wood was completely dissolved within 1 h, forming a homogeneous wood solution.

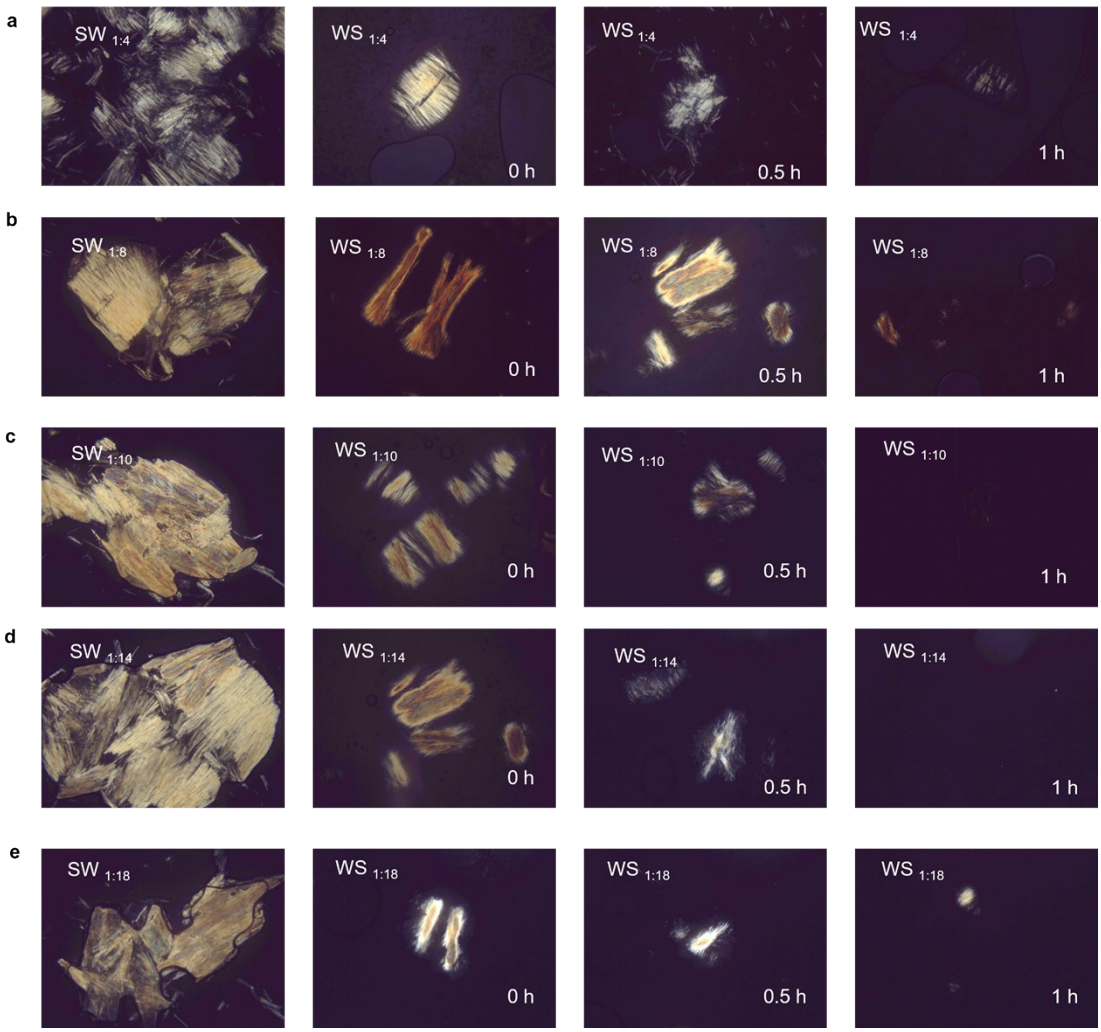

Fig. S3. The effect of the $ZnCl_2$-to-LA molar ratio in DES on the dissolution of wood in $Z_1H_3L_{0.2}$. Optical micrographs show the effect of wood swelling in $ZnCl_2$-LA DES with different $ZnCl_2$:LA molar ratios ((a)1:4, (b)1:8, (c)1:10, (d)1:14 and (e)1:18) on its dissolution behavior in $ZnCl_2 \cdot 3H_2O$ for different time. When the $ZnCl_2$-to-LA molar ratio was adjusted to 1:10, the wood was completely dissolved within 1 h, forming a homogeneous wood solution.

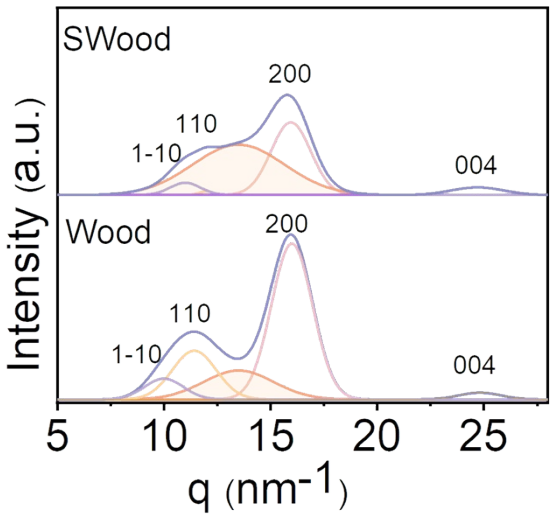

Fig. S4. WAXS profiles comparing untreated Wood and SWood.

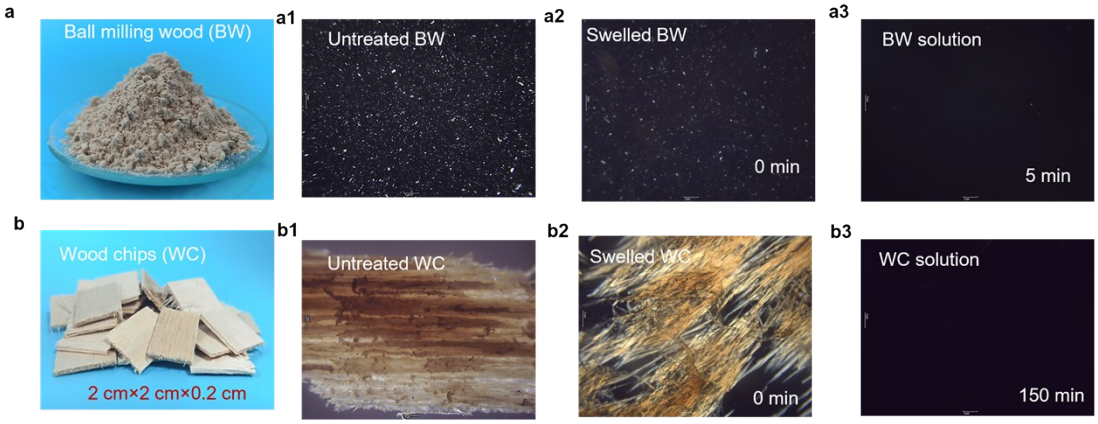

Fig. S5. Dissolution of various sizes wood. (a) Digital photographs of ball-milled wood (BW). (a1) Polarized microscope images of untreated BW, (a2) swelled BW, and (a3) BW solution (c3). (b), Digital photo of wood chip (WC) with a thickness of 0.2 cm and a length and width of 2cm. (b1) Polarized microscope image of untreated WC, (b2) swelled WC, and (b3) WC solution.

Fig. S6. Polarizing light microscope images showing the dissolution process of untreated and swelled fibers for different materials—cotton, hemp, bamboo, and straw—at room temperature over varying time intervals with images captured at specific time points. For each material, the untreated and swelled states are presented, followed by images of fibers in solution at intervals from the start of dissolution: cotton (0, 5, 15, and 30 min), hemp (0, 10, 30, and 60 min), bamboo (0, 30, 90, and 120 min), and straw (0, 30, 90, and 180 min).

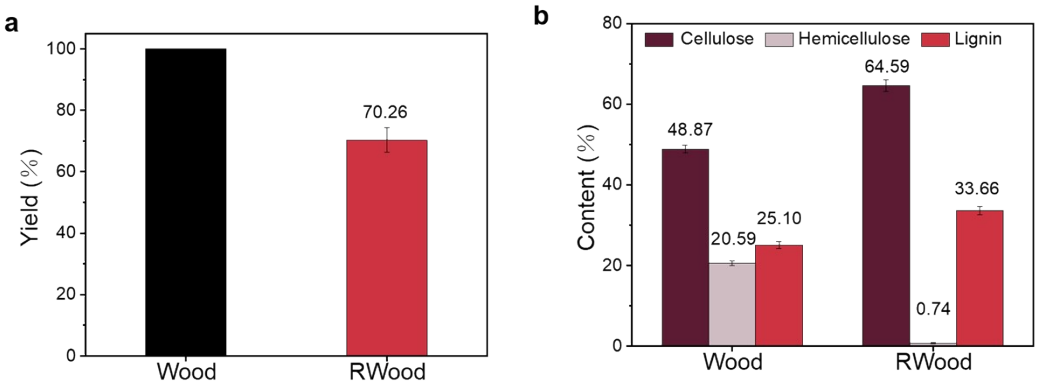

Fig. S7. (a) The yield and (b) component content of wood and Rwood.

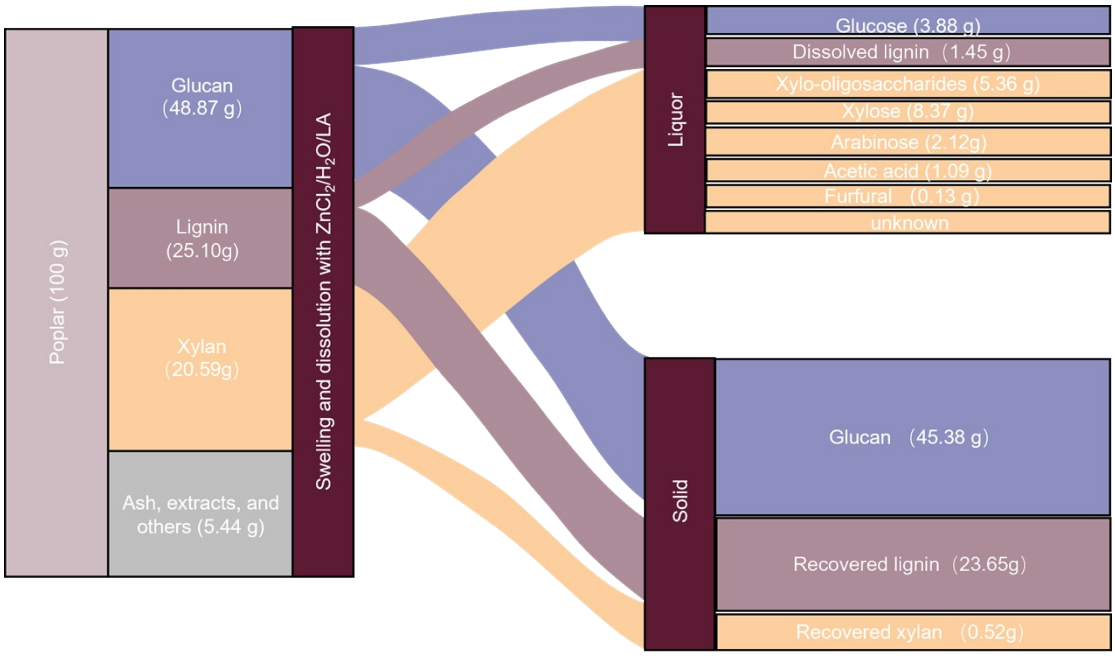

Fig. S8 Schematic diagram and mass balance of the proposed wood dissolution process.

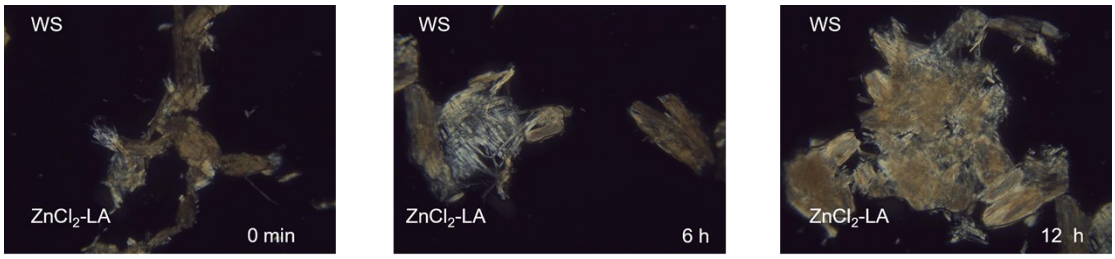

Fig. S9. Polarizing microscope of wood at different times in $ZnCl_2$-LA. Birefringence did not disappear after 12 h, indicating that the wood was not dissolved in $ZnCl_2$-LA.

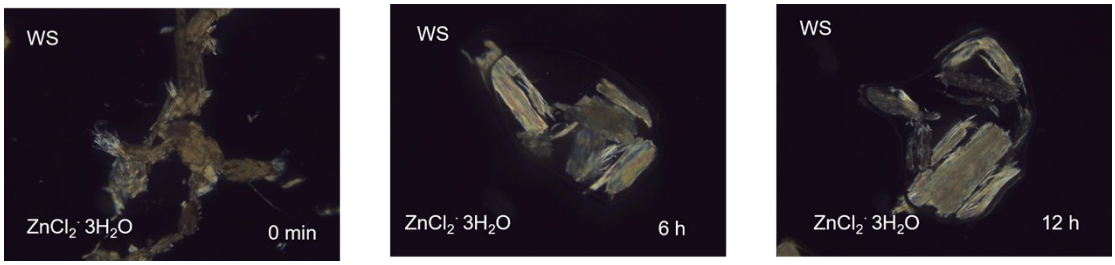

Fig. S10. Polarizing microscope of wood at different times in $ZnCl_2 \cdot 3H_2O$. Birefringence did not disappear after 12 h, indicating that the wood was not dissolved in $ZnCl_2 \cdot 3H_2O$.

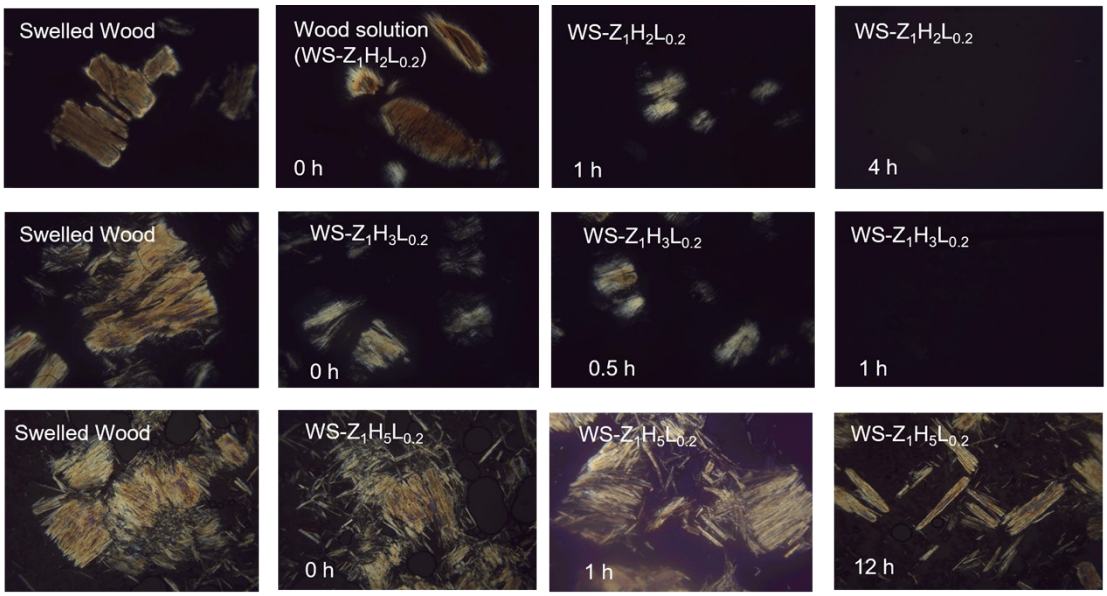

Fig. S11. Optical micrographs illustrate the time-dependent dissolution of wood pre-swollen in $ZnCl_2$-LA DES within $ZnCl_2$ solutions of varying hydration states ($ZnCl_2 \cdot 2H_2O$, $ZnCl_2 \cdot 3H_2O$, $ZnCl_2 \cdot 5H_2O$).

.....

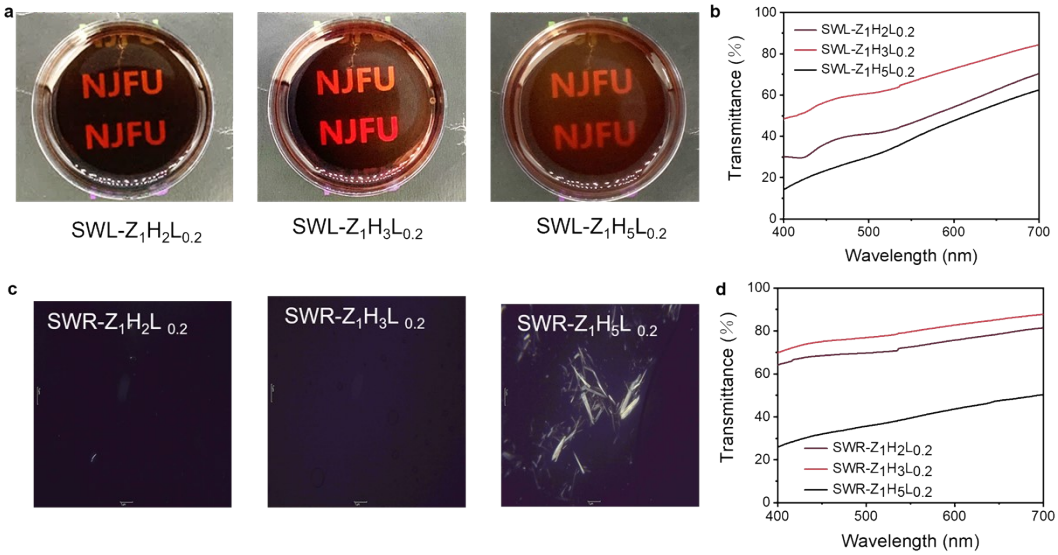

Fig. S12. (a) Digital photos and (b) UV curves of SWL-$Z_1H_2L_{0.2}$, SWL-$Z_1H_3L_{0.2}$, and SWL-$Z_1H_5L_{0.2}$. (c) Digital photos and (d) UV curves of SWR-$Z_1H_2L_{0.2}$, SWR-$Z_1H_3L_{0.2}$, and SWR-$Z_1H_5L_{0.2}$.

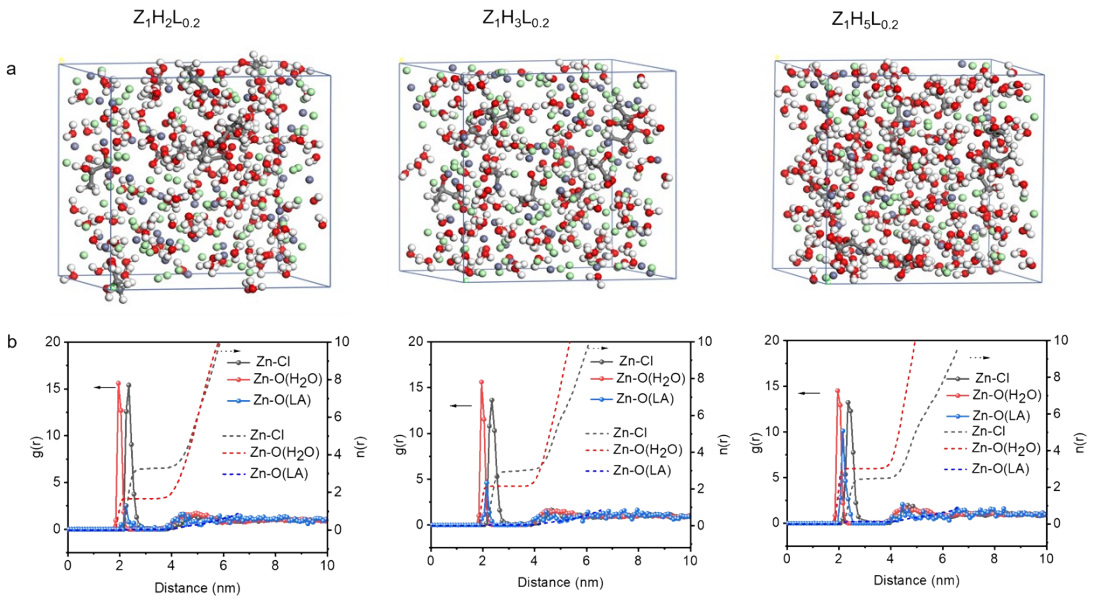

Fig. S13. Molecular dynamics screenshots (b) radial distribution function and coordination number of $Z_1H_2L_{0.2}$, $Z_1H_3L_{0.2}$, $Z_1H_5L_{0.2}$.

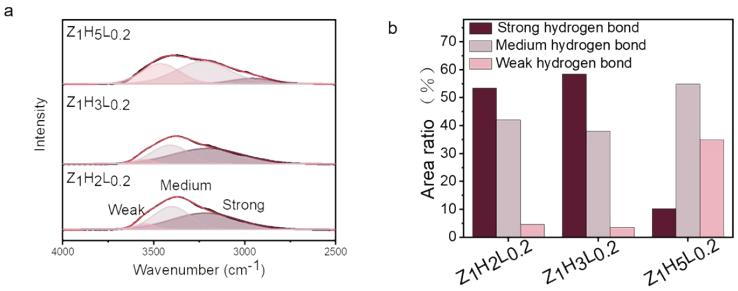

Fig. S14. (a) The fitting of O-H stretching vibration in the FTIR spectra of $Z_1H_2L_{0.2}$, $Z_1H_3L_{0.2}$, and $Z_1H_5L_{0.2}$. (b) The proportion of medium-strong hydrogen bonds, medium-strong hydrogen bonds and weak hydrogen bonds

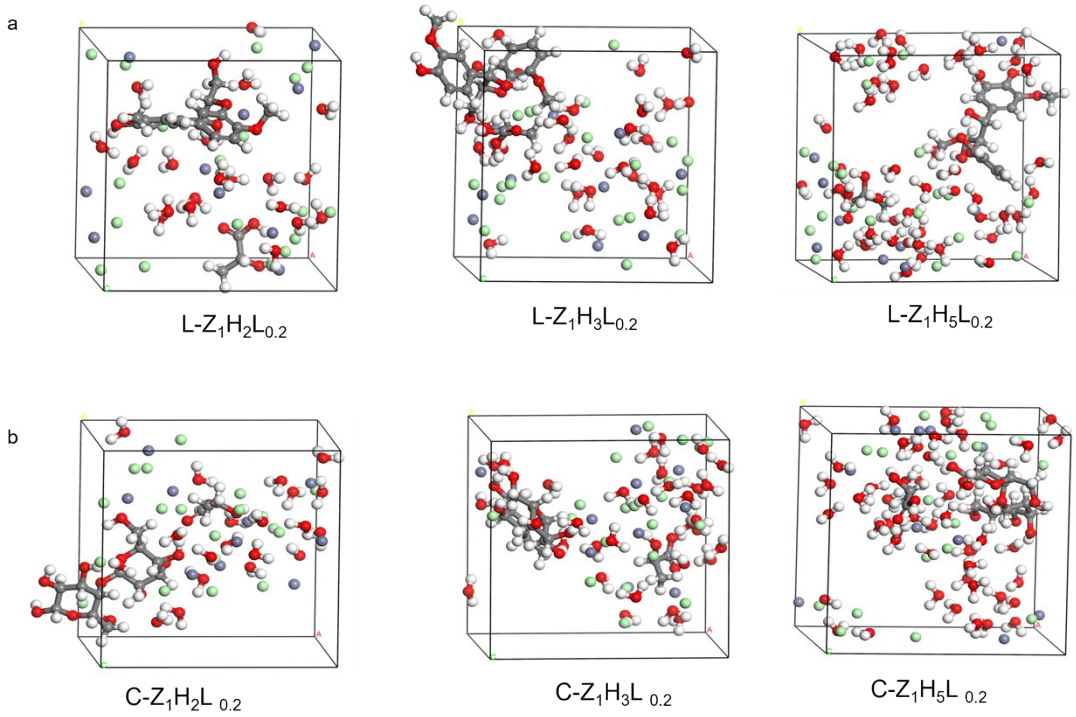

Fig. S15. The conformations of (a) lignin and (b) cellulose after dissolution in $Z_1H_2L_{0.2}$, $Z_1H_3L_{0.2}$, and $Z_1H_5L_{0.2}$.

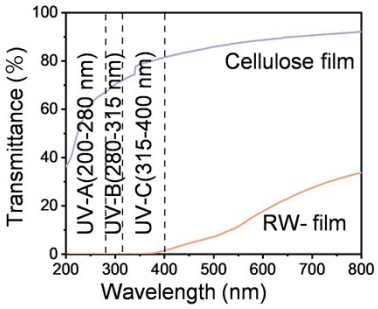

Fig. S16. Transmission spectra of cellulose and wood films, highlight the UV shielding capabilities of the materials. The cellulose film exhibits higher transmittance across the spectrum, particularly in the UV region, compared to the wood film, which shows more effective UV blocking properties.

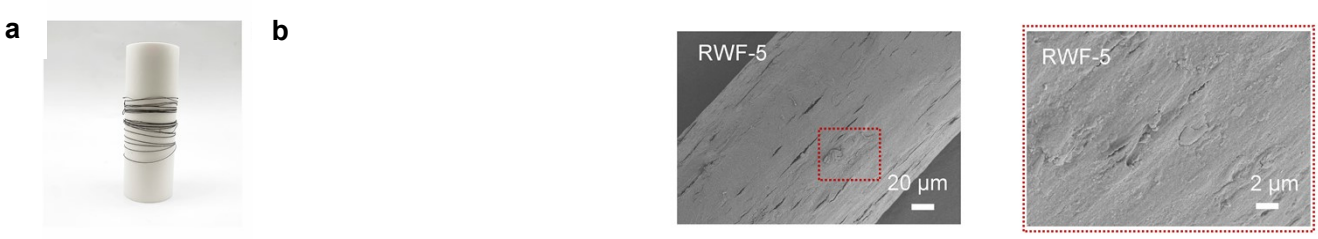

Fig. S17. (a) Digital photographs of RWF. **(b)** SEM image of RWF.

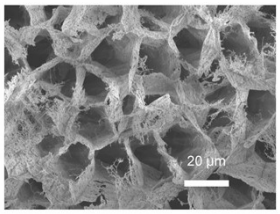

Fig. S18. SEM image revealing the porous microstructure of the regenerated wood aerogel.

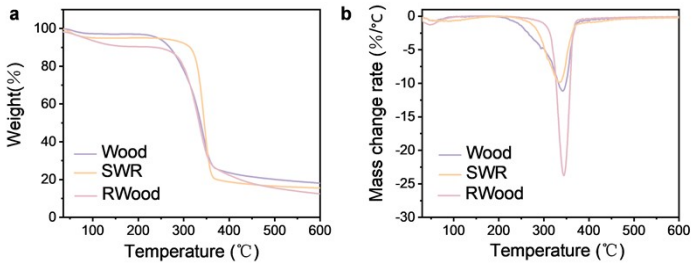

Fig. S19. Thermal stability analysis of Wood, SWR, and RWood. (a) TGA curves. (b) DTG curves.

References

1. P. Chen, Y. Y. Li, Y. Nishiyama, S. V. Pingali, H. M. O'Neill, Q. Zhang and L. A. Berglund, *Nano Letters*, 2021, **21**, 2883-2890.
2. Z. Tong, W. Wang, S. Zeng, Y. Sun, J. Meng, Y. Liu, Q. Xia and H. Yu, *Green Chemistry*, 2022, **24**, 8760-8769.
3. K. S. Salem, N. K. Kasera, M. A. Rahman, H. Jameel, Y. Habibi, S. J. Eichhorn, A. D. French, L. Pal and L. A. Lucia, *Chemical Society Reviews*, 2023, **52**, 6417-6446.
4. L. Zhang, J. Chu, S. Gou, Y. Chen, Y. Fan and Z. Wang, *Industrial Crops and Products*, 2021, **171**.
5. Z. Xie, X. Zhao, C. Huang, C. Lai and Q. Yong, *Chemical Engineering Journal*, 2025, **524,** 113927.
6. D. Tian, J. Hu, R. P. Chandra, J. N. Saddler and C. Lu, *ACS Sustainable Chemistry & Engineering*, 2017, **5**, 2702-2710.
7. Y. Chen, Y. Jiang, D. Tian, J. Hu, J. He, G. Yang, L. Luo, Y. Xiao, S. Deng, O. Deng, W. Zhou and F. Shen, *International Journal of Biological Macromolecules*, 2020, **164**, 3038-3047.
8. J. B. Ocreto, W.-H. Chen, A. P. Rollon, H. Chyuan Ong, A. Pétrissans, M. Pétrissans and M. D. G. De Luna, *Chemical Engineering Journal*, 2022, **445**, 136733.
9. H. Sun, Z. Jin, C. Yang, R. L. C. Akkermans, S. H. Robertson, N. A. Spenley, S. Miller and S. M. Todd, *Journal of Molecular Modeling*, 2016, **22,47**.
10. S. Nosé, *Molecular Physics*, 2006, **52**, 255-268.
11. H. J. C. Berendsen, J. P. M. Postma, W. F. van Gunsteren, A. DiNola and J. R. Haak, *The Journal of Chemical Physics*, 1984, **81**, 3684-3690.
12. S.-Y. Sun, X.-Y. Nie, J. Huang and J.-G. Yu, *Journal of Membrane Science*, 2020, **595**.
13. T. D. Pham, A. Bin Faheem, S. Y. Chun, J. R. Rho, K. Kwak and K. K. Lee, *Advanced Energy Materials*, 2021, **11,** 2003520.
14. Z. Wang, T. Yokoyama, H.-m. Chang and Y. Matsumoto, *Journal of Agricultural and Food Chemistry*, 2009, **57**, 6167-6170.
15. K. kilpeläinen, H. Xie, A. King. M. Granstrom. S. Heikkinen, D. S. Argyropoulos. J. Agric. Food Chem. 2007, **55 (22)**, 9142–9148.
16. Y. Wang, H. Wang, L. Chen, W. Wang, Z. Yang, Z. Xue and T. Mu, *Green Chemistry*, 2023, **25**, 4685-4695.
17. N. Sun, M. Rahman, Y. Qin, M. L. Maxim, H. Rodríguez and R. D. Rogers, *Green Chemistry*, 2009, **11**.
18. Y. Nishiwaki-Akine and T. Watanabe, *Green Chemistry*, 2014, **16**, 3569-3579.